Cytoplasmic Domain of Zebrafish Myelin Protein Zero: Adhesive Role Depends on β-Conformation

XiaoYang Luo,* Hideyo Inouye,* Abby A. R. Gross,* Marla M. Hidalgo,* Deepak Sharma,* Daniel Lee,* Robin L. Avila,* Mario Salmona,† and Daniel A. Kirschner*

*Department of Biology, Boston College, Chestnut Hill, Massachusetts; and †Department of Molecular Biochemistry and Pharmacology, Istituto di Ricerche Farmacologiche "Mario Negri", Milan, Italy

ABSTRACT Solution spectroscopy studies on the cytoplasmic domain of human myelin protein zero (P0) (hP0-cyt) suggest that H-bonding between β-strands from apposed molecules is likely responsible for the tight cytoplasmic apposition in compact myelin. As a follow-up to these findings, in the current study we used circular dichroism and x-ray diffraction to analyze the same type of model membranes previously used for hP0-cyt to investigate the molecular mechanism underlying the zebrafish cytoplasmic apposition. This space is significantly narrower in teleosts compared with that in higher vertebrates, and can be accounted for in part by the much shorter cytoplasmic domain in the zebrafish protein (zP0-cyt). Circular dichroism measurements on zP0-cyt showed similar structural characteristics to those of hP0-cyt, i.e., the protein underwent a $\beta \rightarrow \alpha$ structural transition at lipid/protein (L/P) molar ratios >50, and adopted a β-conformation at lower L/P molar ratios. X-ray diffraction was carried out on lipid vesicle solutions with zP0-cyt before and after dehydration to study the effect of protein on membrane lipid packing. Solution diffraction revealed the electron-density profile of a single membrane bilayer. Diffraction patterns of dried samples suggested a multilamellar structure with the β-folded P0-cyt located at the intermembrane space. Our findings support the idea that the adhesive role of P0 at the cytoplasmic apposition in compact myelin depends on the cytoplasmic domain of P0 being in the β-conformation.

INTRODUCTION

Multilamellar myelin of the internode is formed by spiral wrapping of the glial cell process around the axon, followed by extrusion of the interposing cytoplasm and extracellular fluid. Consequently, there are extensive intermembrane contacts at both the cytoplasmic and extracellular appositions in myelin. Exposure to a variety of physical-chemical treatments demonstrates the relative stability of the cytoplasmic apposition compared to the lability of packing at the extracellular apposition (1). Swelling and compaction at the extracellular apposition as a function of pH and ionic strength can be largely accounted for by the Derjaguin-Landau-Verwey-Overbeek theory of colloid stability (2,3), which provides a formalism for describing the balance between repulsive electrostatic and attractive van der Waals forces in intermembrane interactions (4). In addition, it has been proposed that specific electrostatic interactions involving histidine residues modulate the adhesive interface between the extracellular domains of *trans*-acting protein zero (P0) (3,5,6), which is the major protein in the peripheral nervous system (PNS). Mutations in the gene for this protein result in hereditary sensory and motor neuropathies often with packing defects of myelin membranes (7–9). Such studies indicate the central role of P0 in myelin compaction, membrane adhesion, and myelin function.

By contrast with our understanding of intermembrane interactions at the extracellular apposition, the molecular mechanism accounting for the stable, narrow cytoplasmic apposition of mature myelin has not yet been explained. For peripheral myelin of both higher vertebrates (such as mouse) and lower vertebrates (such as zebrafish), the cytoplasmic apposition is very stable over a wide range of pH and ionic strength (2,10,11), suggesting that electrostatic interactions are unlikely to be the major force in maintaining the membrane packing at this apposition. Our recent solution studies on human P0-cyt in model membranes composed of phosphatidylcholine (PC)/phosphatidylserine (PS) vesicles showed a novel conformational transition from β-sheet to α-helix at lipid/protein (L/P) molar ratios >50, the level in mature PNS myelin, whereas the protein secondary structure remains unchanged in vesicles composed of only negatively charged lipid PS or phosphatidylinositol (PI) (12). These results strongly suggest that the cytoplasmic apposition of PNS myelin may be stabilized, in part, by H-bonding between the β-strands of the *trans*-interacting hP0-cyt but not by the electrostatic interaction between this domain and negatively charged lipids. Furthermore, immature myelin, in which the internodal myelin is still uncompacted, may contain an α-helical form of hP0-cyt, which is anchored via the single Trp residue located near the N-terminus of this domain. This α-helical form of hP0-cyt might facilitate formation of a channel or serve in signal transduction during critical stages of myelination (12).

Submitted May 14, 2007, and accepted for publication July 17, 2007.

Address reprint requests to D. A. Kirschner, Biology Department, Boston College, 140 Commonwealth Ave., Higgins Hall, Chestnut Hill, MA 02467-3811. Tel.: 617-552-0211; Fax: 617-552-2011; E-mail: kirschnd@bc.edu.

Editor: David D. Thomas.

0006-3495/07/11/3515/14 $2.00

doi: 10.1529/biophysj.107.112771

In this study, which is a continuation of the previous one, we used circular dichroism (CD) and the same lipid vesicle system to explore whether a similar L/P-molar-ratio-dependent conformational change occurs for zebrafish P0-cyt (zP0-cyt), whose significantly shorter length likely accounts for its peripheral myelin's narrower cytoplasmic apposition (~24 Å; (13) compared to that in higher vertebrates such as mice (~33 Å; (2,10,11). Additionally, using x-ray diffraction, we sought to investigate the effect of the highly positively charged zP0-cyt on membrane compaction. X-ray diffraction on vesicle solutions containing different amounts of zP0-cyt showed electron-density profiles from a single membrane bilayer, whereas the same samples after dehydration gave a multilamellar structure with similar membrane units but narrower intermembrane space at L/P molar ratios $\leq$50 compared with samples containing no or smaller amounts of protein. Moreover, the x-ray diffraction data showed electron-density elevation at the bilayer surface for dehydrated samples at L/P molar ratios of ~20 and 50, in which zP0-cyt was in a β-conformation, as shown by CD measurements. However, for the dehydrated sample at a L/P molar ratio of ~100, such density elevation was not observed. These results indicate that zP0-cyt in a β-conformation is likely to be localized at the intermembrane space of a multilamellar structure (such as compact myelin), and like hP0-cyt, zP0-cyt may stabilize the cytoplasmic apposition via H-bonding between the β-strands of apposed molecules. Our current model system, therefore, successfully simulated major characteristics of the cytoplasmic apposition in peripheral myelin—the very narrow separation between membrane surfaces and the nonionic interaction between these surfaces.

EXPERIMENTAL PROCEDURES

Sodium dodecyl sulfate (SDS) and 2,2,2-trifluoroethanol (TFE) were obtained from Sigma (St. Louis, MO). Egg PC, brain PS, bovine liver PI, and cholesterol were obtained from Avanti Polar Lipids (Alabaster, AL).

Peptide synthesis

The 32-residue-long zP0-cyt (14) (and the 69-residue hP0-cyt (15); (12)) with free N- and C-termini were synthesized at the Department of Molecular Biochemistry and Pharmacology, Institute for Pharmacological Research ''Mario Negri'', Milano, Italy, using solid-phase peptide synthesis (16). The peptides were purified by reverse-phase HPLC, and their purities were >95% as determined by MALDI-TOF. The sequences for these two polypeptides and their secondary structures as predicted by 3D-PSSM (17) are shown in Fig. 1 *A*.

Preparation of lipid vesicles

The vesicles were prepared according to published procedures (12). Briefly, PS, or PI, or mixtures of PC and PS (molar ratio 12:1) or PC, PS, and cholesterol (molar ratio 62:5:33), were dissolved in pure chloroform and dried under a gentle stream of N_2 gas to form a lipid film, and further dried under high vacuum overnight. The dried lipid film was hydrated in an aqueous buffer to form a lipid suspension. Small unilamellar vesicles (SUVs) were produced by sonicating the lipid suspension in an ice-water bath using an ultrasonic homogenizer equipped with a microtip probe (Cole-Parmer Instrument, Chicago, IL) for ~20 min or until the solution became translucent. Titanium particles shed by the ultrasonic probe into the solution were

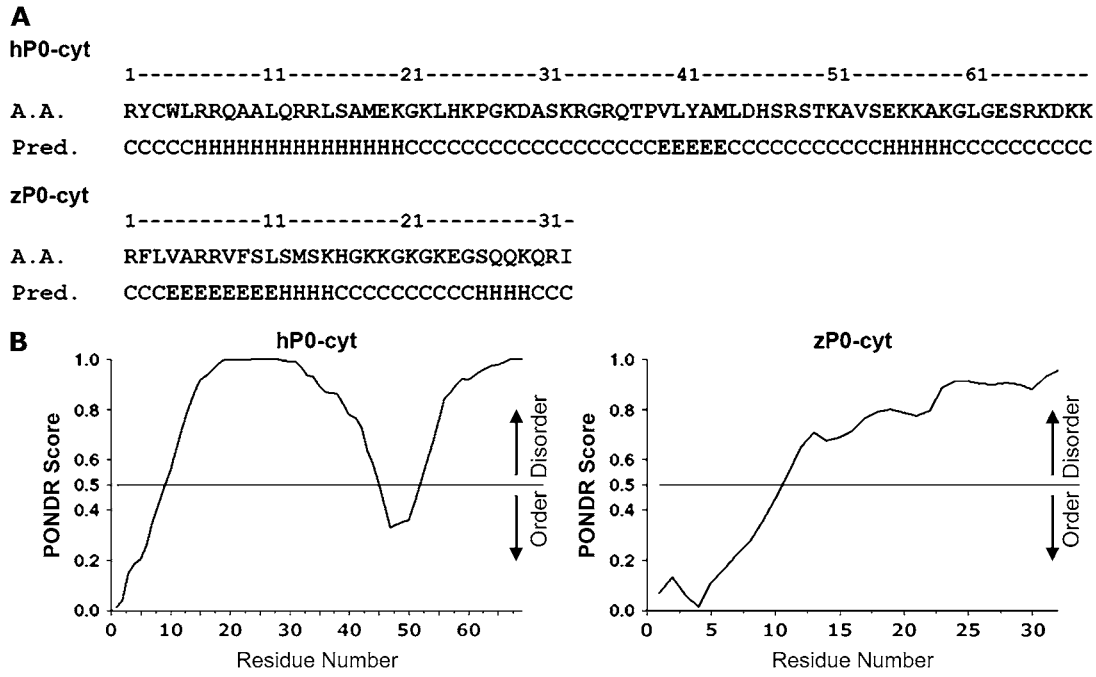

FIGURE 1 Primary sequence, predicted secondary structure, and predicted disorder of cytoplasmic domain for human and zebrafish P0. (*A*) Amino acid sequence (*A.A.* (14,15)) and secondary structure prediction (*Pred.* (17)) for hP0-cyt (*above*) and zP0-cyt (*below*). *H*, α-helix; *E*, β-strand; and *C*, random coil. (*B*) Predictions of intrinsic structural disorder of hP0-cyt and zP0-cyt generated by PONDR VL-XT (28).

removed by centrifugation. Total lipid concentration in lipid vesicles ranged from 0.1 to 4 mg/ml for CD measurements and 25 mg/ml for x-ray diffraction.

Circular dichroism spectroscopy

All CD samples were prepared in phosphate-buffered saline (PBS) unless otherwise noted. All data were acquired on an AVIV Model 202 circular dichroism spectropolarimeter (Lakewood, NJ), located in the Chemistry Department at Boston College. Samples of vesicles made of PS or PI alone were made in 0.5 mM Tris-HCl, pH 7.4, instead of PBS, to avoid turbidity caused by protein-induced vesicle aggregation. Spectra were recorded in a 0.1-cm-pathlength rectangular quartz cell at 25°C from 260 nm to 195 nm with 1-nm increments and an averaging time of 1 s/data point. For all CD measurements, zP0-cyt concentration was 30 μM. Seven scans for each sample were averaged, smoothed using the inverse exponential method and plotted using SigmaPlot 2001 (Systat Software, Richmond, CA). All CD spectra were corrected for buffer, detergent, or lipid vesicle contributions. Ellipticity is reported as mean molar residue ellipticity (MRE) in deg cm^2 dmol^{-1}. The fractional contents of secondary structures (α, β, and random coil) were calculated using the software CDPro; and the wavelength used for the analysis was 195–260 nm, with 29 soluble proteins constituting the reference set (18). The per-residue molar absorption units of circular dichroism $\Delta\varepsilon$, which is measured in mdeg M^{-1} cm^{-1} is related to MRE according to $\Delta\varepsilon$ = MRE/3298. First, the calculated fractions of each secondary-structure content from all three programs included in CDPro (CONTIN, SELCON3, and CDSSTR) were averaged, then the averaged fractions of $H(r)$ (regular α-helix) and $H(d)$ (distorted α-helix), $S(r)$ (regular β-strand) and $S(d)$ (distorted β-strand), and T (turns) and U (unordered) were used to give the overall content of α, β, and random structure, respectively.

X-ray diffraction

Freshly prepared vesicle solutions at constant lipid (PC/PS = 12:1) concentration of 26.4 mM with or without different amounts of hP0-cyt or zP0-cyt peptide were aspirated into thin-wall glass or quartz capillary tubes 0.5 mm in diameter (Charles Supper, South Natick, MA), which were then sealed with wax and nail polish on both ends. Diffraction experiments were carried out using nickel-filtered, single-mirror focused CuK_α radiation from a fine-line source on a 3.0 kW Rigaku x-ray generator (Rigaku/MSC, The Woodlands, TX) operated at 40 kV by 14 mA. The diffraction patterns were recorded for 1 h using a linear, position-sensitive detector (Molecular Metrology, Northampton, MA). The observed intensity recorded from aqueous buffer (PBS) was subtracted from each sample. The background curve was determined by fitting the intensity minima to a polynomial curve (11). The detector read-out was averaged within a window of 21 pixels to smooth the data.

After x-ray data collection, the samples (in the capillary) were dehydrated at room temperature by evaporation through a tiny hole punched into the wax seal while under a low vacuum generated in a desiccator. Two-dimensional x-ray patterns, in the range of 2–50 Å Bragg spacing, were recorded from the peptides alone and from dehydrated vesicle samples at different L/P molar ratios. We used the Oxford diffraction Xcalibur PX Ultra system (Oxford Diffraction, Concord, MA) located in the laboratory of Dr. Andrew Bohm (Department of Biochemistry, Tufts University, Boston, MA). The CuK_α x-ray beam was generated using an Enhance Ultra, which is a sealed-tube-based system incorporating confocal multilayer optics. The x-ray beam was monochromated and the K_β component was removed by means of the double bounce within the confocal optic. The x-ray beam was focused to an area 0.3 mm × 0.3 mm (full width at half-maximum at detector position). A two-dimensional Onyx CCD detector (Oxford Diffraction, Concord, MA) was placed 85 mm from the sample position. The sample-to-detector distance was calibrated using a spherical ylid crystal (molecular formula $C_{10}H_{10}SO_4$) or a cubic alum crystal, according to the information given by the manufacturer. Bragg peaks from silver behenate (58.38-Å period) were used to calibrate the specimen-to-film distance and to calculate the pixel size of the image (121 μm). The active range of the detector was 165 mm, and the two dimensional image (1024 × 1024 pixels; in 2 × 2 binning) was collected using the software CrysAlis (CrysAlis CCD and RED, version 171 (2004), Oxford, UK) and stored in the compressed image format IMG. The output readout, stored on a hard disk, was linear with x-ray intensity to ~1.3×10^5. Exposure times ranged from 150 to 300 s. The diffraction image in JPEG format supplied by CrysAlis RED was translated to TIFF, then displayed by NIH Image (available at http://rsb.info.nih.gov/nih-image/), and further analyzed by FIT2D. The scattering intensity from the blank capillary tube was recorded by shifting the capillary tube vertically so that the x-ray incident beam went through empty capillary tube. This intensity was then subtracted from those of the dehydrated vesicles and lyophilized or vapor-hydrated peptide samples.

Electron-density distribution

The lamellar phase of lipid vesicle solutions showed a continuous intensity curve of $I_{obs}(R)$, where R is the reciprocal coordinate of a one-dimensional lattice. The structure factor $F(R)$ is related to $I_{obs}(R)$ according to $F^2(R) = R^n I_{obs}(R)$ where $n = 1$ is the geometrical correction of the observed line-focused intensity and $n = 2$ is the point-focused intensity. For the low-angle intensity, the polarization factor was chosen as one. The electron-density profile $\rho(r)$, determined for the lamellar structure, where the r axis is assumed to be normal to the flat membrane surface, is given by

$$\rho(r) = 2\int_{r=0}^{\infty} \pm|F(R)|\cos(2\pi rR)dR.$$

For numerical calculation, R was defined by h/D, where h is an integer and D is a large number (e.g., 1000 Å). Then,

$$\rho(r) = \frac{F(0)}{D} + \frac{2}{D}\sum_{h=1}^{h_{max}} \pm|F(h/D)|\cos(2\pi rh/D).$$

Some samples showed powder diffraction with distinct Bragg peaks that may correspond to multiple Miller indices. The extraction of the structure amplitudes was performed as described previously (19,20). In brief, the procedure was as follows. 1), Our initial atomic fraction coordinates (x,y,z) were for β-keratin, which gives a typical β-crystallite structure (21). 2), The structure factors were calculated using the initial coordinates and the observed lattice constants. 3), The observed amplitudes $|F_{obs}(h,k,l)|$ were combined with the calculated phases $\Phi(h,k,l)$, and the residual between the observed and calculated amplitudes were determined. 4), Finally, the electron-density distribution was computed from the observed amplitudes and calculated phases according to $\rho(x,y,z) = \sum_{hkl}|F_{obs}(h,k,l)|\Phi(h,k,l)\exp[i2\pi(hx + ky + lz)]$.

RESULTS

zP0-cyt secondary structure depended on concentration of TFE or SDS, and on lipid/protein molar ratio

Far-UV CD spectrum of zP0-cyt suggested a predominant β-sheet structure (<10% α and ~50% β) when the protein was in aqueous buffer (Fig. 2), similar to what was observed for hP0-cyt (Fig. 2 (12)). When TFE or SDS was added to the buffer, a gradual increase of α- and decrease of β-contents in zP0-cyt secondary structure occurred as the relative amount of protein decreased (Fig. 2). Whereas these treatments induce a similar trend of conformational change for hP0-cyt

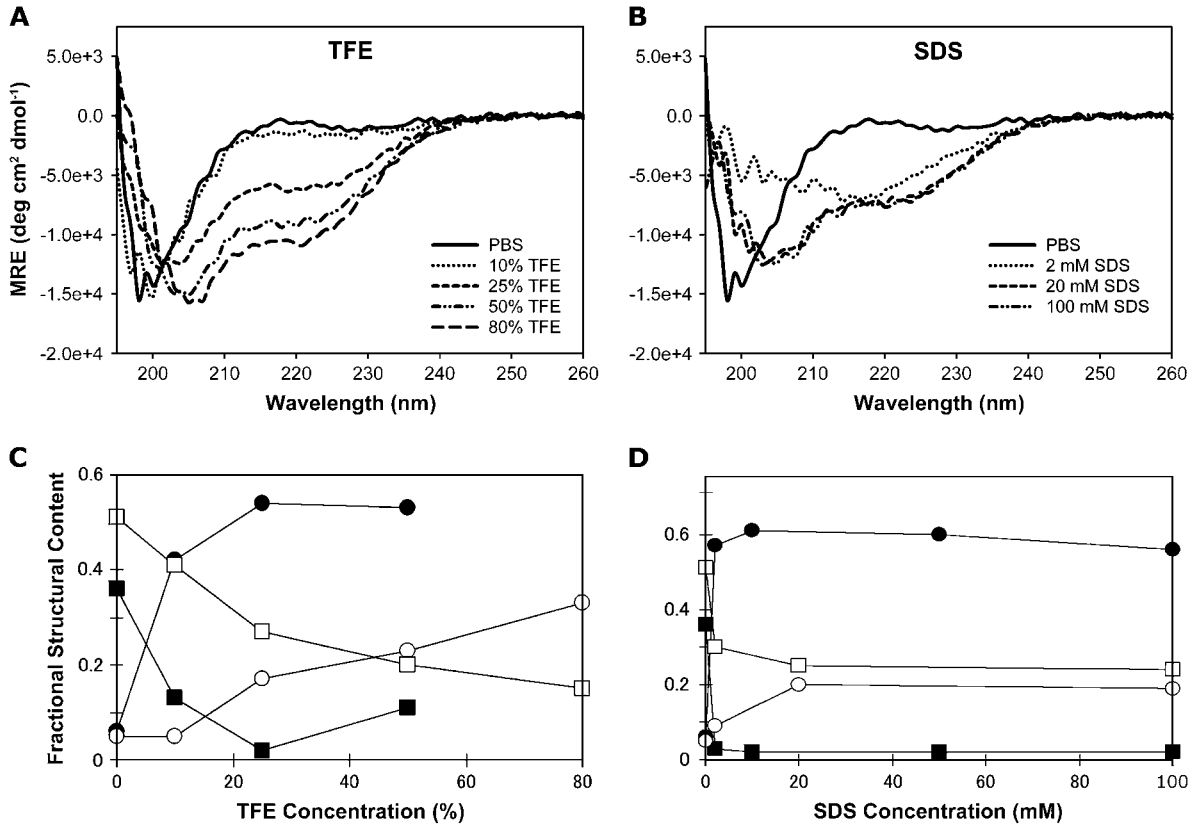

FIGURE 2 CD spectra of zP0-cyt in the presence of different concentrations of (*A*) TFE and (*B*) SDS. Secondary-structure fractions calculated from program CDPro (18) were plotted as a function of concentration of (*C*) TFE and (*D*) SDS. Solid symbols indicate hP0-cyt spectra, and open symbols zP0-cyt spectra. The fractional contents of α and β are shown by circles and squares, respectively.

(12), i.e., an increase of α and decrease of β, the changes in secondary-structure contents of these two peptides were quantitatively different under the same experimental conditions. For example, in 10% TFE, hP0-cyt structure contained $>40\%$ α and $<15\%$ β, whereas zP0-cyt adopted only $\sim 5\%$ α but $>40\%$ β-structures. In 50% TFE, the α-contents were $>50\%$ and $\sim 20\%$, and the β-contents were $\sim 10\%$ and $\sim 20\%$ for hP0-cyt and zP0-cyt, respectively (Fig. 2, *A* and *C*). Similarly, SDS increased α-helical structure for zP0-cyt, but was not as effective as it was for hP0-cyt (Fig. 2, *B* and *D*). These results indicate that the β-structure of zP0-cyt is more resistant to TFE and SDS than that of hP0-cyt.

To study zP0-cyt structure in an environment more closely mimicking the myelin membrane, we utilized the same lipid vesicle system as previously used for hP0-cyt (12). Specifically, CD spectra were acquired for PC/PS vesicle samples at different L/P molar ratios (Fig. 3 *A*). zP0-cyt and hP0-cyt underwent a similar $\beta \rightarrow \alpha$ structural transition, i.e., α-content increased and β-content decreased, at L/P molar ratios >50. However, the conformational change of zP0-cyt was not as pronounced as that of hP0-cyt (Fig. 3, *A* and *C*), which was similar to that observed when the proteins were mixed with different amounts of TFE or SDS (Fig. 2).

CD spectra of zP0-cyt in vesicles containing additional cholesterol showed a similar trend in conformational change as a function of L/P molar ratio compared with that of the protein in vesicles without cholesterol (Fig. 3, *B* and *D*). This result is different from what was previously observed for hP0-cyt, which shows an early $\beta \rightarrow \alpha$ transition at an L/P molar ratio of ~ 20 and a decrease in both α- and β-contents at higher L/P molar ratios (12).

Secondary structure of zP0-cyt relatively unaffected by negatively charged lipids in vesicles

As zP0-cyt, like hP0-cyt, has a large positive charge, we used vesicles composed of only acidic lipid (PS or PI) to test for potential charge effects on protein conformation. zP0-cyt maintained a nearly constant secondary structure (mainly β) in samples at different PS or PI concentrations, similar to what was observed for hP0-cyt under the same conditions (Fig. 4). These data suggest that the negative charge of vesicle lipids was unlikely to be responsible for the observed $\beta \rightarrow \alpha$ structural transition of either zP0-cyt or hP0-cyt at L/P molar ratios >50 in the vesicle solutions.

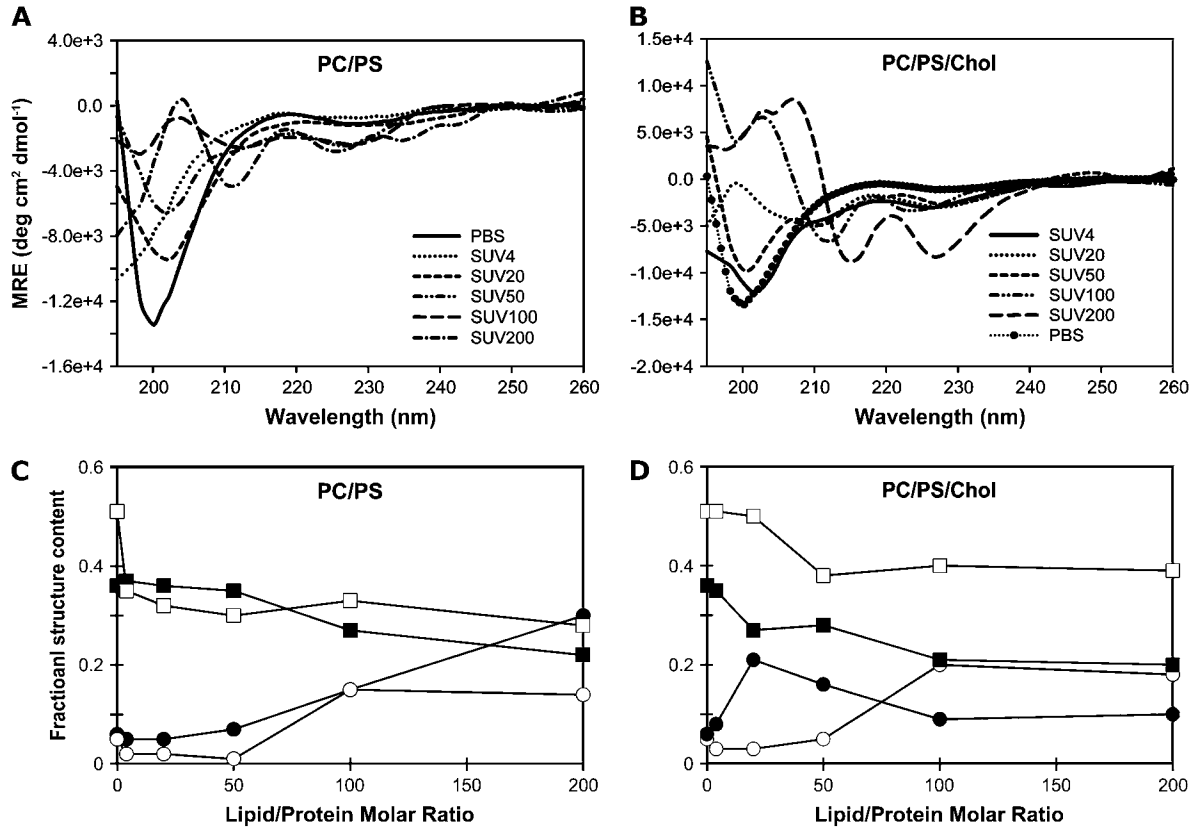

FIGURE 3 CD spectra of zP0-cyt in lipid vesicles composed of (*A*) PC and PS, and (*B*) PC, PS, and cholesterol. The lipid/protein molar ratios 4, 20, 50, 100, and 200 are designated as SUV4, SUV20, SUV50, SUV100, and SUV200, respectively. Secondary-structure fractions calculated from program CDPro (18) were plotted as a function of lipid/protein molar ratio for vesicles made of (*C*) PC/PS and (*D*) PC/PS/cholesterol. hP0-cyt is represented by solid symbols and zP0-cyt by open symbols. The fractional contents of α and β are shown by the circles and squares, respectively.

Solution x-ray scattering from SUVs consistent with single membrane bilayer

To verify that the lipid vesicle system we used for the CD measurements was, indeed, composed of single-membrane-bilayer vesicles, x-ray diffraction patterns for vesicle solutions containing different amounts of hP0-cyt or zP0-cyt (Fig. 5, *A* and *B*) were analyzed. The scattering intensity of the aqueous buffer (PBS) showed a nearly constant intensity in the observed reciprocal range of 0.01–0.07 Å^{-1} (not shown). The intensities of lipid samples with different amounts of peptide (hP0-cyt or zP0-cyt) were similar to those from the control lipid vesicles without peptides. All diffraction patterns showed a diffuse band having a maximum at ~0.02 Å^{-1} and minima at ~0.01 and 0.04 Å^{-1} (Fig. 5, *A–D*), which are similar to the expected Fourier transform for a single bilayer profile (Fig. 5, *E* and *F* (22)). The transform for a membrane pair, by contrast, has maxima at ~0.014 and ~0.024 Å^{-1}, and a minimum at ~0.02 Å^{-1}.

Using π as a phase angle for the loop expected for a symmetric single membrane (Fig. 5, *E* and *F*), the structure factors in the range 0.011–0.04 Å^{-1} sampled by 1000 Å was derived for lipids alone and for the mixture of lipids and proteins. The electron-density projections along the axis normal to the lamellar plane were indistinguishable from one another at this resolution, indicating little or no effect of protein on the bilayer profile (Fig. 5, *G* and *H*).

Dried vesicles were multilamellar

To more closely simulate the multilamellar structure of the compact myelin, which is relatively anhydrous, vesicle solutions containing different amounts of zP0-cyt were dehydrated and examined using x-ray diffraction at both low- and wide-angles. Diffraction patterns of the dried samples at different L/P molar ratios showed a very strong, ~50-Å reflection, much weaker 25-Å and 13-Å reflections at low angles, and a wide-angle, broad band at 4.6-Å spacing (Fig. 6, *A–F*, and Table 1). The low-angle reflections, which were indexed as $h = 1$, 2, and 4, indicated a multilamellar structure having a period of ~50 Å. zP0-cyt at an L/P molar ratio of 100 gave Bragg orders $h = 1$, 2, and 4 for a structure with a 49-Å period. At L/P = 50, the lamellar period decreased to 44 Å and an additional Bragg reflection (indexed as $h = 3$) was observed. At L/P = 20, similar

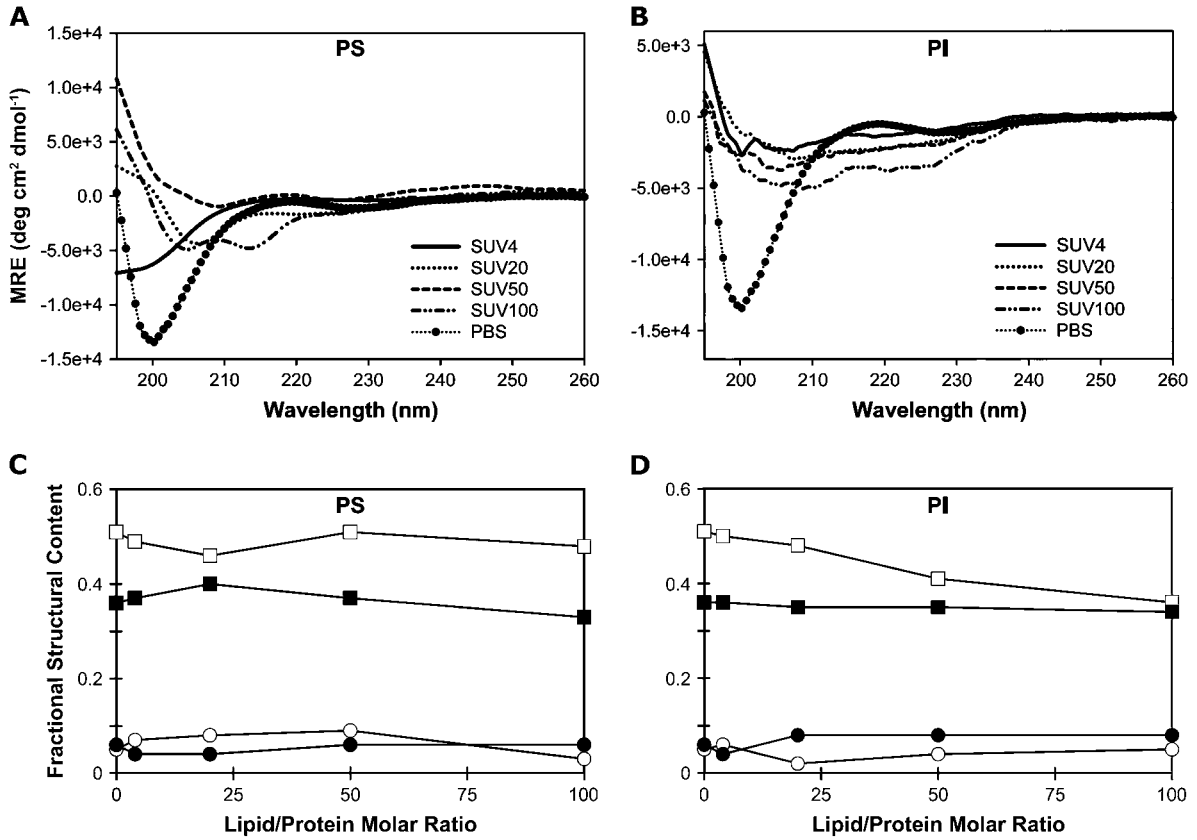

FIGURE 4 CD spectra of zP0-cyt in SUVs made of only negatively charged lipid (*A*) PS or (*B*) PI. The lipid/protein molar ratios 4, 20, 50, and 100 are designated as SUV4, SUV20, SUV50, and SUV100, respectively. Secondary-structure fractions, calculated using the program CDPro (18), were plotted as a function of lipid/protein molar ratio for vesicles made of (*C*) PS and (*D*) PI. hP0-cyt is represented by solid symbols, and zP0-cyt by open symbols. The fractional contents of α and β are shown by the circles and squares, respectively.

reflections ($h = 1, 2, 3$, and 4) were observed. The broad 4.6-Å wide-angle reflection (not shown) was consistent with the hydrocarbon chains being disordered. A similar spacing is observed for peptides in the β conformation, where ~4.7 Å corresponds to the distance between hydrogen-bonded β-strands (21).

When plotted as a function of the reciprocal coordinate, the observed structure factors were found to sample a single, continuous Fourier transform (Fig. 6 *G*), indicating similar membrane units with variable widths of space between them. The electron-density profiles were calculated with the assigned signs of either + or – for the structure factors (Fig. 6 *H*). The calculated profiles were similar to that from the atomic coordinates for crystallized phosphatidylethanolamine (PE) (23,24). Whereas the membrane profile for the dried vesicles containing zP0-cyt at an L/P molar ratio of 100 was similar to that for the lipid control, the profiles of samples containing higher concentrations of zP0-cyt (L/P molar ratios of 50 and 20) showed elevated electron density at the membrane surface between bilayers (Fig. 6 *H*, *short arrows*). This higher electron density at the membrane interface likely resulted from zP0-cyt in a β-conformation, which was its predominant structure in vesicle solutions at L/P molar ratios <100.

zP0-cyt and hP0-cyt, when lyophilized or vapor-hydrated, gave x-ray diffraction typical of β-crystallite structures

Lyophilized zP0-cyt and hP0-cyt peptides gave spherically averaged powder patterns that showed three reflections, at Bragg spacings of ~10 Å, 4.6 Å, and 3.8 Å (data not shown). Such reflections are characteristic of β-crystallites with orthogonal unit-cell constants of $a = \sim 9.4$ Å, $b = \sim 6.6$ Å, and $c = \sim 10$ Å, where the a, b, and c axes are in the directions of hydrogen-bonding, chain, and intersheet, respectively (19,21). After vapor hydration (Fig. 7, *A* and *B*), the intersheet reflection at ~10 Å was no longer visible due to the weakening of the intersheet interaction by hydration (e.g., see Fig. 1 in Bond et al. (25) and Fig. 3 *A* in Inouye et al. (26)); however, other distinct reflections became visible at spacings of 4.68 Å, 3.75 Å, 3.12 Å, and 2.69 Å (Fig. 7 *A*, *a–d*, respectively) for hP0-cyt, and at 4.75 Å, 3.72 Å, and 3.08 Å for zP0-cyt (Fig. 7 *B*, *a′–c′*, respectively). The unit

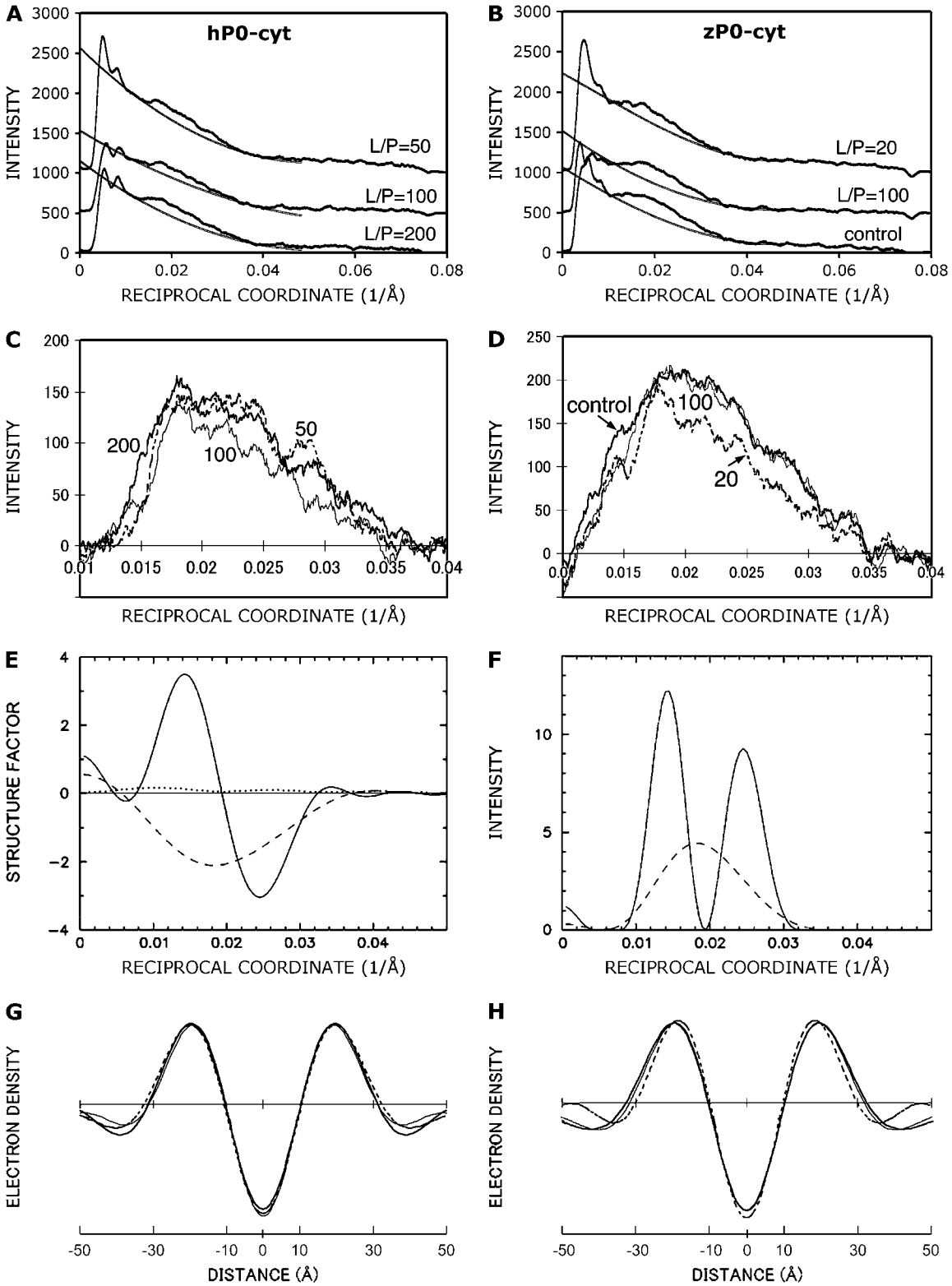

FIGURE 5 X-ray diffraction data (*A–D*), analysis of patterns (*E* and *F*), and electron-density profiles (*G* and *H*) for vesicle solutions containing protein. Observed x-ray diffraction intensities as a function of reciprocal coordinate (1/Å) for vesicle solutions with (*A*) hP0-cyt and (*B*) zP0-cyt at different L/P molar ratios. Different intensity curves are vertically shifted for clarity. The observed intensity of the lamellar phase for PC/PS vesicles with (*C*) hP0-cyt at L/P molar ratios 200 (*thick line*), 50 (*dashed line*), and 100 (*thin line*), and (*D*) the control (i.e., PC/PS vesicle alone) (*thick line*), with zP0-cyt at L/P molar ratios 20 (*dashed line*) and 100 (*thin line*). The intensity is a read-out of the position-sensitive detector after background subtraction. (*E*) The continuous transform $F(R)$ for a pair of membranes for mouse nerve myelin membranes (on an absolute scale) as a function of reciprocal coordinate in the direction normal to the

cell was orthogonal and its lattice constants were $a = 9.24$ Å, $b = 6.31$ Å, and $c = 9.53$ Å for hP0-cyt, and $a = 9.31$ Å and $b = 6.22$ Å for zP0-cyt.

Because of the predominant β-conformation, the initial set of phases was calculated according to the fractional atomic coordinates reported for β-keratin (19,21) and the observed diffraction pattern for hP0-cyt. The electron-density profiles calculated using the observed hP0-cyt amplitudes and the calculated phases were characteristic of that expected for β-sheets (Fig. 7, *C* and *D*). The microenvironment of zP0-cyt and hP0-cyt molecules in lyophilized or vapor-hydrated powders is similar to that for the cytoplasmic apposition of compact myelin in that both environments are characterized by local, very high concentrations of the protein. Therefore, the β-structures observed from powder diffraction data for both peptides might be closely related to their native structures in the myelin sheath. This possibility is supported by the aforementioned CD experiments on the vesicle solutions (Fig. 3) and x-ray diffraction experiments on the same samples after dehydration (Fig. 6), both of which also indicated potential β-structure of the peptides in compact myelin.

DISCUSSION

Although the sequences and lengths of zP0-cyt and hP0-cyt are quite distinct from one another, our CD data showed an unexpected similarity between these two peptides in terms of their structural characteristics in membrane mimetics. Our results suggest a common mechanism by which these two proteins stabilize their respective cytoplasmic appositions in compact myelin. Negatively charged lipid (PS or PI) alone did not have a noticeable effect on the secondary structures of either hP0-cyt or zP0-cyt, suggesting that electrostatic interactions do not play the primary role in stabilizing the cytoplasmic appositions of PNS myelin from either humans or zebrafish. This notion is in agreement with previous studies that show a remarkable stability of the cytoplasmic appositions in both mouse and zebrafish peripheral myelin (2,11,13). Both proteins adopted primarily a β-structure in PC/PS vesicles at L/P molar ratios $\leq$50, which is the level in mature PNS myelin. This indicates that they both may have the β-conformation in compact myelin, and that H-bonding between β-strands from *trans*-interacting P0-cyt molecules may serve as the major force to stabilize the narrow cytoplasmic apposition.

Biological relevance of L/P-molar-ratio-dependent conformational change

In this study, using a membrane mimetic composed of PC/PS vesicles, we found that zP0-cyt had little change in secondary structure at L/P molar ratios $\leq$50, whereas when the proportion of lipid increased, the structure underwent a $\beta \rightarrow \alpha$ transition. Although the exact lipid and protein content (including P0 and myelin basic protein) is not known for zebrafish (13), the current threshold of $\sim$50 in the L/P molar ratio that effected a structural transition in zP0-cyt suggests that compact myelins in zebrafish and humans have similar L/P molar ratios.

Our x-ray diffraction data from dehydrated lipid vesicles containing different amounts of zP0-cyt suggested that only at L/P ratios $\leq$50 did zP0-cyt become localized at the intermembrane space of multibilayers, and this localization was coupled to a 6-Å decrease in bilayer spacing (Fig. 6 *H*). This is consistent with the proposed adhesive role of β-folded zP0-cyt at the cytoplasmic apposition in compact myelin.

Role of cholesterol in conformation of hP0-cyt versus zP0-cyt

The CD data showed different structural changes between hP0-cyt and zP0-cyt when these two proteins were mixed with PC/PS vesicles containing cholesterol. hP0-cyt underwent a $\beta \rightarrow \alpha$ conformational change at an L/P molar ratio of 20 and a decrease in both β- and α-contents at higher L/P molar ratios (12). Therefore, it appears that cholesterol can interact with hP0-cyt in a concentration-dependent manner: at L/P molar ratios $<$20, cholesterol serves as an α-inducer, and at L/P molar ratios $>$20 as a denaturant for hP0-cyt structure.

A similar effect of cholesterol on the protein folding of zP0-cyt, however, was not observed. Cholesterol did not seem to induce any additional change in zP0-cyt structure compared with the protein in vesicles lacking cholesterol but having the same L/P molar ratios (Fig. 3, *C* and *D*).

FIGURE 5 (Continued).
membrane surface (*solid line*). Original intensity data were from Bragg peaks for a myelin period of 216 Å (22). For absolute scaling, we used an electron-density level of the water layer of 0.3347 $e/Å^3$, an exclusion length of 136 Å, and an average electron density within the exclusion length of 0.343 $e/Å^3$. The electron-density distribution of a pair of membrane $\rho(r)$ is written for an asymmetric unit $\sigma(r)$ as $\rho(r) = \sigma(r)*\delta(r-u)+\sigma(-r)*\delta(r+u)$, where * is a convolution operation, and u is the packing distance from the origin where the asymmetric unit is positioned. The Fourier transform of $\sigma(r)$ gives $a(R) + ib(R)$. The terms $a(R)$ and $b(R)$ are shown as *dashed* and *dotted lines*, respectively. $F(R)$ is related to these terms according to $F(R) = 2[a(R)\cos(2\pi uR) - b(R)\sin(2\pi uR)]$. (*F*) The corresponding intensity for a pair of membranes is $|F(R)|^2$ (*solid line*) and for a single membrane, $a^2(R)+b^2(R)$ (*dashed line*). Note that the intensity maximum and minimum for a single membrane are at 0.02 $Å^{-1}$ and 0.04 $Å^{-1}$, respectively. (*G*) Electron-density distribution on a relative scale as a function of distance (Å) for vesicles with hP0-cyt at L/P molar ratios of 50 (*thick line*), 100 (*dashed line*), and 200 (*thin line*). (*H*) Electron-density distribution for vesicle control (*thin line*), and vesicles with zP0-cyt at L/P molar ratios of 50 (*thick line*) and 100 (*dashed line*). The Lorentz type correction factor $RI(R)$ was chosen by taking into consideration the integration along the slit direction in the line-collimated pattern.

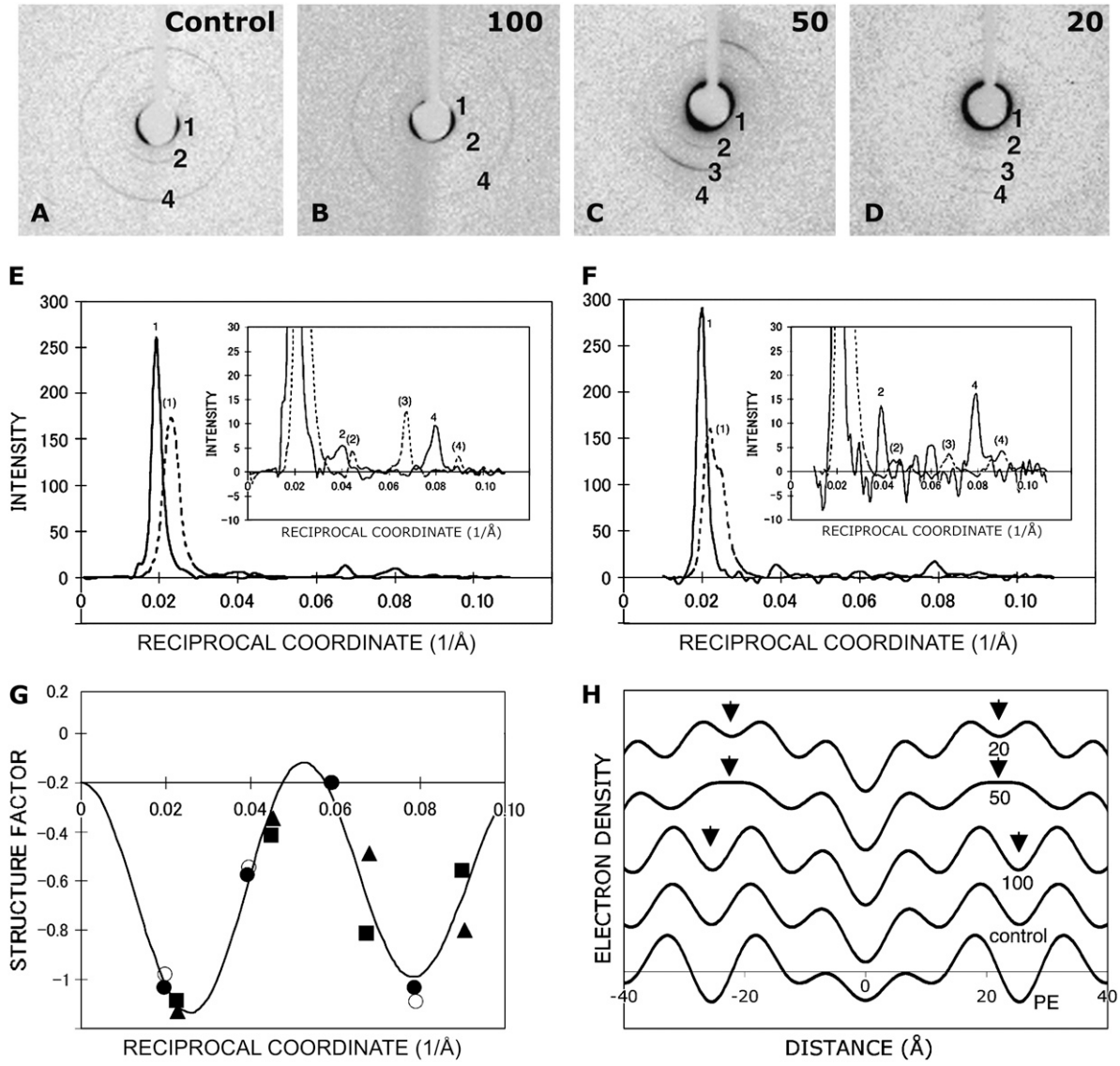

FIGURE 6 X-ray diffraction data, analysis of patterns, and electron-density profiles for vesicles dried from solution. (*A–D*) X-ray diffraction patterns from the dried control vesicles and samples with zP0-cyt at L/P molar ratios of 100, 50, and 20 after subtracting the intensity of the empty capillary tubes. The low-angle reflection indices are indicated beside the corresponding reflections. The diffraction patterns were taken using the Oxford Xcalibur system (specimen-to-film distance, 85 mm; exposure times, 150 s). (*E*) Observed x-ray diffraction intensities of dried PC/PS vesicle without protein (*solid line*) or with zP0-cyt at L/P molar ratio of 50 (*dashed line*) after background subtraction as a function of reciprocal coordinate ($Å^{-1}$) in the membrane stacking direction. The intensity was normalized so that the area under the curve was one. The indices of the lamellar periods (50.9 Å for the control and 44.5 Å for L/P molar ratio of 50; in parentheses) are indicated above the Bragg peaks. (*F*) Observed x-ay diffraction intensities for dried samples of zP0-cyt at L/P molar ratio = 100 (*solid line*) and L/P molar ratio = 20 (*dashed line*). The periods were 50.6 Å and 44.2 Å, respectively. (*G*) Structure factors as a function of reciprocal coordinate (1/Å) for the dried vesicle control ($d = 50.9$ Å (*solid circle*)), samples of zP0-cyt at L/P molar ratio of 100 ($d = 50.6$ Å (*open circle*)), 50 ($d = 44.5$ Å (*solid square*)), and 20 ($d = 44.2$ Å (*solid triangle*)). The structure amplitudes were scaled according to $\sum F^2(h)/d = \sum h^2 I_{obs}(h)/d = 0.03$. The continuous curve was an average of the Fourier transform of the electron-density profiles of the aforementioned samples. (*H*) Electron-density profiles as a function of distance along the multibilayer stacking direction for the dried PC/PS vesicle control ($d = 50.9$ Å), zP0-cyt samples at L/P molar ratio = 100 ($d = 50.6$ Å), 50 ($d = 44.5$ Å), and 20 ($d = 44.2$ Å). The electron-density projection along the stacking direction was calculated from the crystallographic data of PE ($d = 48.9$ Å (23,24)). Bilayer boundaries are indicated by arrows.

This observation may be explained if zP0-cyt interacts with cholesterol in a manner different from that of hP0-cyt. Alternatively, zP0-cyt and hP0-cyt may interact with cholesterol in similar ways but the structure of the former is more resistant to the effect of cholesterol. This latter possibility is consistent with the CD data that showed a less dramatic structural change for zP0-cyt than for hP0-cyt when the protein was mixed with the same amount of membrane-mimicking compounds or vesicle lipids (Figs. 2 and 3). As native myelin contains a significant amount of cholesterol,

TABLE 1 Structure factors of the lamellar, dehydrated lipid vesicles containing zP0-cyt at different L/P molar ratios

Sample	Lipid PC/PS control	L/P = 100	L/P = 50	L/P = 20	PE crystal
Lamellar period d (Å)	50.9	50.6	44.5	44.2	48.9
$F(1)$	−0.832	−0.778	−0.886	−0.928	−0.544
$F(2)$	−0.375	−0.344	−0.213	−0.143	−0.524
$F(3)$	0.000	0.000	−0.612	−0.288	0.579
$F(4)$	−0.832	−0.890	−0.359	−0.600	−0.748

The structure factors $F(h)$ were scaled according to $\sum_{h=1}^{4} F^2(h)/d = 0.03$, where h is the order of the reflection and d is the lamellar period.

our CD data may be particularly relevant to the conformation of zP0-cyt and hP0-cyt in the native, cholesterol-rich membranes.

Molecular model of zP0-cyt at apposed cytoplasmic surfaces

Although the sequences of zP0-cyt and hP0-cyt differ greatly from one another, both peptides have a very large positive charge at neutral pH (pI = 10.88 and 12.02, respectively) and extremely low hydrophobicity, which are the two major characteristics of so-called ''intrinsically disordered proteins'' (27). Indeed, both proteins were predicted to contain large percentages of disordered regions (69% for zP0-cyt and 78% for hP0-cyt) when analyzed by ''Predictor of Naturally Disordered Regions'' (PONDR; Fig. 1 *B* (28)).

The CD spectra showed ~50% random coil for both zP0-cyt and hP0-cyt in aqueous buffer (Fig. 2), which was consistent with the predicted large proportion of disordered sequences. The predicted secondary-structure propensities from 3D-PSSM (17) were 25% α and 25% β for zP0-cyt, and 29% α and 7% β for hP0-cyt (Fig. 1 *A*). These values for β-contents were smaller than those measured by CD (i.e., ~50% for zP0-cyt and ~40% for hP0-cyt). However, the fact that the net predicted ($\alpha + \beta$)-content was similar to that measured suggests that some residues in α may change to β depending on the specific environment—for example, in the presence of added lipids, detergents, organic solvents, and salts (Fig. 2).

The narrower cytoplasmic space in zebrafish peripheral myelin (~24 Å (13)) compared to that of higher vertebrates (e.g., mouse, ~33 Å (2,10,11)) is consistent with the substantially fewer amino acid residues in zP0-cyt (32) versus twice as many in the others (e.g., 69 in hP0-cyt). As we predicted using 3D-PSSM (17), the three-dimensional structure of hP0-cyt has two antiparallel β-chains linked by a reverse turn (12). These short $\beta-$structures might nucleate the β-folding of hP0-cyt, whose homophilic interaction via the H-bonding between β-chains may account for the stable, narrow cytoplasmic apposition in compact myelin (12). A similar tertiary structure prediction for zP0-cyt also showed a short β-strand at residues 7–19 near the N-terminal side of zP0-cyt (Fig. 8). Like the short antiparallel β-chains predicted for hP0-cyt, this short β-strand in zP0-cyt might serve as the core structure to facilitate the folding of the entire domain when in an appropriate environment. 3D-PSSM modeling also showed that within the cytoplasmic space of compact myelin, *trans*-oriented zP0-cyt molecules likely interact with each other via H-bonding between the predicted β-strands, which are oriented parallel to the membrane surface and with the hydrogen-bonding direction being along the membrane stacking direction. Surface localization of β-folded zP0-cyt at the intermembrane space is also consistent with the electron-density profiles calculated from the x-ray diffraction patterns of the dried, multilamellar lipid samples (Fig. 6 *H*).

The stacking of the imidazole rings of His-16 and His-16′ from apposing zP0-cyt molecules could contribute to the homophilic interaction at the cytoplasmic apposition. In this model, the His/His′ interaction may be further enhanced by the proximity of Lys-19 (29), which, by lowering the pK_a of His-16, would stabilize the deprotonated form at physiological pH (Fig. 8). Supporting the potential importance of this interaction is the finding that the hP0 missense mutation Lys-236-Glu, corresponding to residue 57 in hP0-cyt, is causative for peripheral neuropathy Charcot-Marie-Tooth disease Type 2 (30), perhaps owing to disruption of the histidine stacking. The sequence containing this substitution (KKAKG, residues 56–60) is homologous with KKGKG (residues 18–22) in zP0-cyt and is near His-16. Thus, these corresponding regions in human and zebrafish may be closely involved in stabilizing the H-bonding between the apposed β-chains.

Large positive charge of P0-cyt has physiological implications

The attachment of water-soluble proteins (or protein domains) to the membrane surface is an important process in cell signaling. Membrane binding facilitates proper protein-protein and protein-substrate interaction. Many integral membrane proteins have, in the cytoplasmic domains, clusters of basic residues (31) that facilitate the attachment of the protein to the membrane interface via electrostatic interactions, often in combination with protein acylation (32–36). It is likely that these basic residues sense the local electric potential produced by negatively charged phospholipids (37), which are preferentially located on the cytoplasmic surface of the membrane (38,39). It has been reported that both protein acylation and electrostatic interactions between the positively charged domains and negatively charged membrane lipids are necessary for membrane association of proteins, e.g., myristoylated alanine-rich C-kinase substrate (MARCKS (40) and the Src tyrosine kinases (41). Phosphorylation within the basic domains of these proteins disrupts the electrostatic interactions and dissociates the proteins from the membrane interface, and therefore could serve as an electrostatic switch to modulate the protein-membrane association (42).

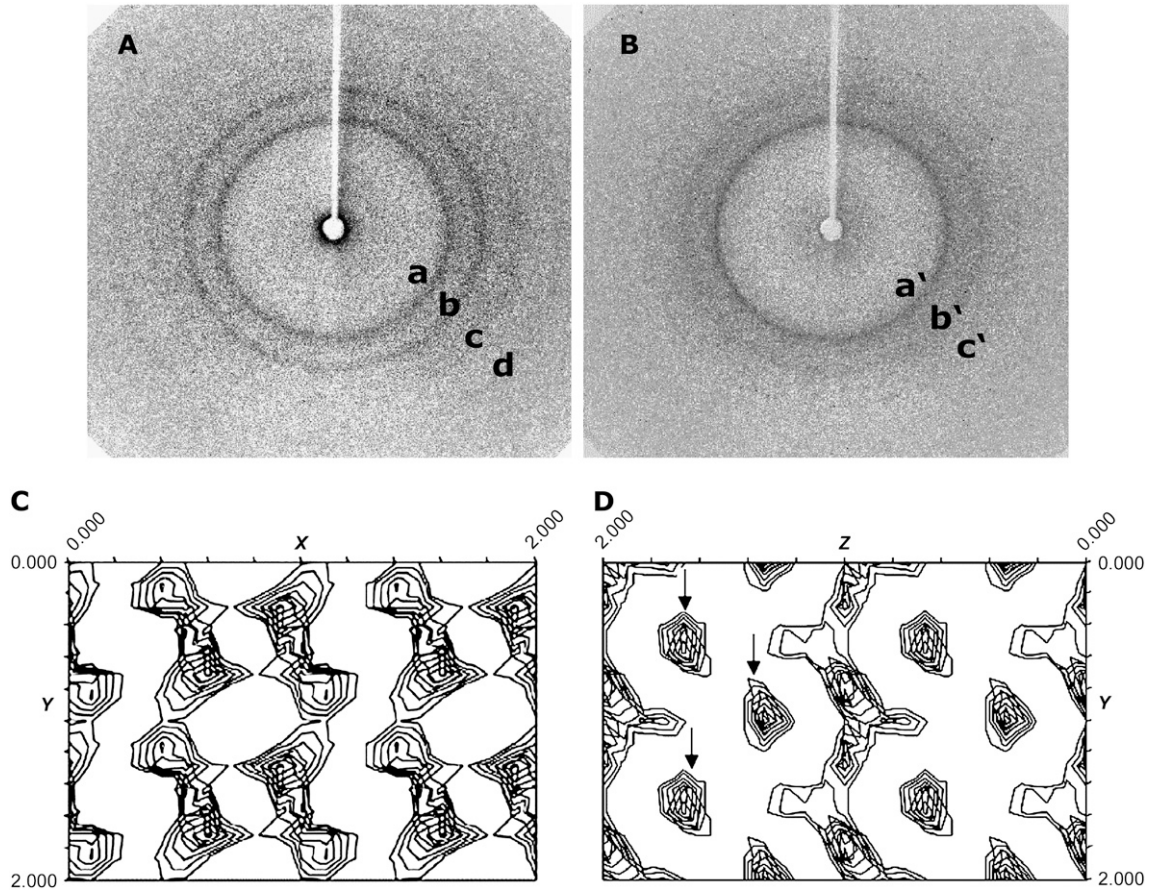

FIGURE 7 X-ray diffraction and electron-density projections for cytoplasmic domains of human and zebrafish P0 after vapor hydration of lyophilized peptide. (*A* and *B*) X-ray diffraction patterns of vapor-hydrated hP0-cyt (*A*) and zP0-cyt (*B*) after subtracting the intensity from empty capillary tubes. Reflections are labeled as described in the text. The diffraction patterns were recorded for 150 s each using the Oxford Xcalibur system with a specimen-to-film distance of 85 mm. The original image was enhanced to show weaker reflections. The inner two strong rings are the 4.6-Å and 3.7-Å reflections of an orthogonal lattice, where $a = 9.24$ Å, $b = 6.31$ Å, and $c = 9.53$ Å for hP0-cyt, and $a = 9.31$ Å and $b = 6.22$ Å for zP0-cyt. (*C* and *D*) Electron-density projections for vapor-hydrated hP0-cyt along the H-bonding direction (*C*) and along the intersheet direction (*D*). The chain direction (*b* axis) is vertical in both *C* and *D*, whereas the H-bonding direction (*a* axis) is horizontal in *C* and the intersheet direction (*c* axis) is horizontal in *D*. These profiles were calculated from the observed intensity (in *A*) and the calculated phases of β-keratin (21). Both *C* and *D* contain two unit cells, i.e., *2a* (horizontal) and *2b* (vertical) in *A*, and *2c* (horizontal) and *2b* (vertical) in *B*, respectively. Note that the β-chains are H-bonded along the *x*-direction in *A*, and that new peaks in the intersheet space in *B* (*arrows*) correspond to the side chains.

Consistent with hP0-cyt's proposed signal transduction role during myelin development (reviewed in (43)), this domain shows striking similarities to the above-mentioned signaling proteins—i.e., large net positive charge, acylation on a Cys residue (44,45), and phosphorylation/dephosphorylation dynamics (46). For this reason, P0 might achieve its membrane attachment in a similar manner, as follows: 1), the protein is initially attracted to the membrane interface through electrostatic interactions with negatively charged lipids, although the latter do not seem to play a significant role in the conformational change of hP0-cyt in PC/PS vesicles at L/P molar ratios >50 ((12) and this study); 2), after membrane binding, the fatty acyl chain might be inserted into the hydrocarbon regions of the membrane bilayer, serving as a membrane anchor to secure the protein at the appropriate orientation and facilitate proper protein-protein, protein-membrane, and protein-cytoskeleton interactions (47); and 3), dephosphorylation events might be needed for stronger protein-membrane associations. Although electrostatic interactions and acylation might both be needed for proper membrane attachment of P0 from higher vertebrates, electrostatic interactions alone might be sufficient for both membrane targeting and strong membrane association with zP0-cyt, as this domain lacks Cys and Tyr residues (Fig. 1).

Physiological and phylogenetic implications of β-folded P0-cyt

Despite the pronounced difference in the sequences of zP0-cyt and hP0-cyt, this study showed that they likely adopt a potentially similar $\beta-$structure that is oriented on the membrane surface of the cytoplasmic apposition in compact

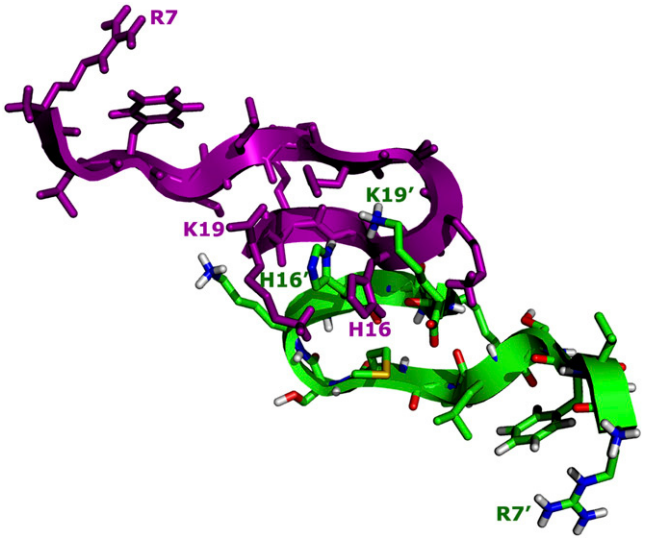

FIGURE 8 Molecular model and proposed homophilic binding interface of zP0-cyt residues 7–19 predicted using 3D-PSSM (17). Note the stacking of the imidazole rings of His-16 and His-16′, and the proximity of Lys residues.

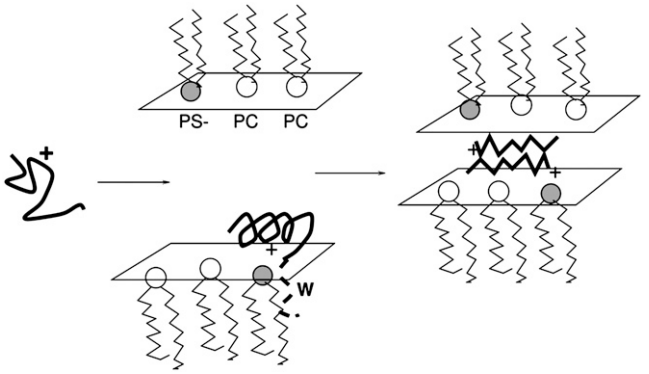

FIGURE 9 Schematic of the model system described here suggests a mechanism in compact myelin for P0-cyt-induced membrane compaction at the cytoplasmic apposition. When myelin is uncompacted, P0-cyt is in an α-helical conformation with its single Trp (*W*) residue serving as a membrane anchor. As the protein assumes more β-conformation and its positive side chains interact with negatively charged lipid headgroups, the cytoplasmic surfaces become more closely apposed. The β-strands are parallel to, and the hydrogen-bonds normal to, the membrane bilayer surfaces.

myelin. This observation can only be explained by the importance of such β-structure in membrane compaction. It is conceivable that a β-sheet structure that is flat on the membrane surface can be reasonably accommodated into the narrow cytoplasmic apposition, and at the same time can account for the invariance of this apposition over a wide range of pH and ionic strength (2,11,13). Therefore, a common mechanism of PNS myelin compaction at its cytoplasmic surface via P0-cyt might have been conserved through evolution. At early stages of myelination, P0-cyt might be α-helical to facilitate the signal transduction events that are crucial for the myelin membrane synthesis and assembly. As more P0 molecules are incorporated into the myelin membrane, P0-cyt starts to fold into a β-structure and the larger overall positive charge of the accumulating P0-cyt molecules increasingly neutralizes the negative charge of the lipid headgroups. Next, the van der Waals attractions from the apposing membrane lipid molecules and H-bonding of β-strands from the *trans*-interacting P0-cyt molecules collectively bring together the facing membranes at the cytoplasmic apposition. During this process, the dynamic phosphorylation/dephosphorylation events in P0-cyt (48) may fine-tune the cytoplasmic apposition by modifying the secondary structure of P0-cyt through change in its net charge. Finally, myelin becomes completely compacted, and H-bonding between the *trans*-located P0-cyt molecules stabilizes the compaction at the cytoplasmic apposition (Fig. 9).

Our simple model system using PC/PS/cholesterol with or without human and zebrafish P0 cytoplasmic domain was found to account for the narrow separation between the membrane surfaces and its nonionic interaction. From our spectroscopic and x-ray small-angle scattering data, and molecular modeling, we proposed a core sequence within P0-cyt in which short β-strands would nucleate folding of the domain and stabilize the apposition via *trans* intermolecular H-bonding. Potential modulators of this interaction are specific residues within hP0-cyt including Thr-37, Ala-42, Lys-57, and Arg-65 (numbered in the complete sequence of processed protein as T216, A221, K236, and R244) that are known missense mutation sites in human peripheral neuropathies (Swiss-Prot variant P25189 (49)). Our data also indicate that specific lipid headgroups interact with the residues in the core β-strands. In summary, the study presented here should not only assist in our understanding of the phylogenetic development of P0's function at the cytoplasmic apposition in PNS compact myelin, but should also provide a simple, yet informative approach for conducting similar structural studies on other important myelin proteins. Studies on P0-cyt with differing sequences from other species, e.g., avian and elasmobranch, or transgenic mice having defined amino acid substitutions, would provide ways to test features of the mechanistic model set forth in this article.

We are grateful to Dr. Andrew Bohm (Department of Biochemistry, Tufts University, Boston, MA) for kindly granting us access to their x-ray diffraction facility, and to the Chemistry Department of Boston College for providing the circular dichroism spectropolarimeter. We also thank one of the anonymous reviewers for suggesting a particular sequence homology between human and zebrafish P0-cyt domains.

M.S. was supported by the European Union within the frame of Neuroprion and Heteroprion networks (contract No. FOOD-CT-2004-506579), Negri-Weizmann Foundation (2006), the Italian Ministry of University and Research (FIRB protocol RBNE03PX83, 2005), and Fondazione Cariplo11 (Project Genoproteomics of Age Related Disorders, 2006). The Kirschner Lab acknowledges institutional support from Boston College.

REFERENCES

1. Kirschner, D. A., and A. E. Blaurock. 1992. Organization, phylogenetic variations and dynamic transitions of myelin structure. *In* Myelin: Biology and Chemistry. R. E. Martenson, editor. CRC Press, Boca Raton, FL. 3–78.
2. Inouye, H., and D. A. Kirschner. 1988. Membrane interactions in nerve myelin. I. Determination of surface charge from effects of pH and ionic strength on period. *Biophys. J.* 53:235–245.
3. Inouye, H., and D. A. Kirschner. 1988. Membrane interactions in nerve myelin: II. Determination of surface charge from biochemical data. *Biophys. J.* 53:247–260.
4. Ninham, B. W., and V. A. Parsegian. 1971. Electrostatic potential between surfaces bearing ionizable groups in ionic equilibrium with physiologic saline solution. *J. Theor. Biol.* 31:405–428.
5. Shapiro, L., J. P. Doyle, P. Hensley, D. R. Colman, and W. A. Hendrickson. 1996. Crystal structure of the extracellular domain from P0, the major structural protein of peripheral nerve myelin. *Neuron.* 17:435–449.
6. Wells, C. A., R. A. Saavedra, H. Inouye, and D. A. Kirschner. 1993. Myelin P0-glycoprotein: predicted structure and interactions of extracellular domain. *J. Neurochem.* 61:1987–1995.
7. Kirschner, D. A., K. Szumowski, A. A. Gabreels-Festen, J. E. Hoogendijk, and P. A. Bolhuis. 1996. Inherited demyelinating peripheral neuropathies: relating myelin packing abnormalities to P0 molecular defects. *J. Neurosci. Res.* 46:502–508.
8. Warner, L. E., M. J. Hilz, S. H. Appel, J. M. Killian, E. H. Kolodry, G. Karpati, S. Carpenter, G. V. Watters, C. Wheeler, D. Witt, A. Bodell, E. Nelis, C. Van Broeckhoven, and J. R. Lupski. 1996. Clinical phenotypes of different MPZ (P0) mutations may include Charcot-Marie-Tooth type 1B, Dejerine-Sottas, and congenital hypomyelination. *Neuron.* 17:451–460.
9. Wrabetz, L., M. D'Antonio, M. Pennuto, G. Dati, E. Tinelli, P. Fratta, S. Previtali, D. Imperiale, J. Zielasek, K. V. Toyka, R. L. Avila, D. A. Kirschner, A. Messing, M. L. Feltri, and A. Quattrini. 2006. Different intracellular pathomechanisms produce diverse *MPZ*-neuropathies in transgenic mice. *J. Neurosci.* 26:2358–2368.
10. Avila, R. L., H. Inouye, R. Baek, X. Yin, B. D. Trapp, M. L. Feltri, L. Wrabetz, and D. A. Kirschner. 2005. Structure and stability of internodal myelin in mouse models of hereditary neuropathy. *J. Neuropathol. Exp. Neurol.* 64:976–990.
11. Inouye, H., J. Karthigasan, and D. A. Kirschner. 1989. Membrane structure in isolated and intact myelins. *Biophys. J.* 56:129–137.
12. Luo, X., D. Sharma, H. Inouye, D. Lee, R. L. Avila, M. Salmona, and D. A. Kirschner. 2007. Cytoplasmic domain of human myelin protein zero likely folded as β-structure in compact myelin. *Biophys. J.* 92: 1585–1597.
13. Avila, R. L., B. R. Tevlin, J. P. Lees, H. Inouye, and D. A. Kirschner. 2007. Myelin structure and composition in zebrafish. *Neurochem. Res.* 32:197–209.
14. Schweitzer, J., T. Becker, C. G. Becker, and M. Schachner. 2003. Expression of protein zero is increased in lesioned axon pathways in the central nervous system of adult zebrafish. *Glia.* 41:301–317.
15. Hayasaka, K., K. Nanao, M. Tahara, W. Sato, G. Takada, M. Miura, and K. Uyemura. 1991. Isolation and sequence determination of cDNA encoding the major structural protein of human peripheral myelin. *Biochem. Biophys. Res. Commun.* 180:515–518.
16. De Gioia, L., C. Selvaggini, E. Ghibaudi, L. Diomede, O. Bugiani, G. Forloni, F. Tagliavini, and M. Salmona. 1994. Conformational polymorphism of the amyloidogenic and neurotoxic peptide homologous to residues 106–126 of the prion protein. *J. Biol. Chem.* 269:7859–7862.
17. Kelley, L. A., R. M. MacCallum, and M. J. Sternberg. 2000. Enhanced genome annotation using structural profiles in the program 3D-PSSM. *J. Mol. Biol.* 299:499–520.
18. Sreerama, N., and R. W. Woody. 2004. On the analysis of membrane protein circular dichroism spectra. *Protein Sci.* 13:100–112.
19. Inouye, H., P. E. Fraser, and D. A. Kirschner. 1993. Structure of β-crystallite assemblies formed by Alzheimer β-amyloid protein analogues: analysis by x-ray diffraction. *Biophys. J.* 64:502–519.
20. Nguyen, J. T., H. Inouye, M. A. Baldwin, R. J. Fletterick, F. E. Cohen, S. B. Prusiner, and D. A. Kirschner. 1995. X-ray diffraction of scrapie prion rods and PrP peptides. *J. Mol. Biol.* 252:412–422.
21. Fraser, R. D. B., and T. P. MacRae. 1973. Conformation in Fibrous Proteins and Related Synthetic Polypeptides. Academic Press, New York.
22. Inouye, H., H. Tsuruta, J. Sedzik, K. Uyemura, and D. A. Kirschner. 1999. Tetrameric assembly of full-sequence protein zero myelin glycoprotein by synchrotron x-ray scattering. *Biophys. J.* 76:423–437.
23. Elder, M., P. Hitchcock, R. P. Mason, and G. G. Shipley. 1977. A refinement and analysis of the crystallography of the phospholipids 1,2-dilauroyl-DL-phosphatidylethanolamine and some remarks on lipid-lipid and lipid-protein interactions. *Proc. R. Soc. A. (Lond.).* 354: 157–170.
24. Inouye, H., F. S. Domingues, A. M. Damas, M. J. Saraiva, E. Lundgren, O. Sandgren, and D. A. Kirschner. 1998. Analysis of x-ray diffraction patterns from amyloid of biopsied vitreous humor and kidney of transthyretin (TTR) Met30 familial amyloidotic polyneuropathy (FAP) patients: axially arrayed TTR monomers constitute the protofilament. *Amyloid.* 5:163–174.
25. Bond, J. P., S. P. Deverin, H. Inouye, O. M. el-Agnaf, M. M. Teeter, and D. A. Kirschner. 2003. Assemblies of Alzheimer's peptides Aβ 25–35 and Aβ31–35: reverse-turn conformation and side-chain interactions revealed by X-ray diffraction. *J. Struct. Biol.* 141:156–170.
26. Inouye, H., D. Sharma, W. J. Goux, and D. A. Kirschner. 2006. Structure of core domain of fibril-forming PHF/Tau fragments. *Biophys. J.* 90:1774–1789.
27. Uversky, V. N., J. R. Gillespie, and A. L. Fink. 2000. Why are ''natively unfolded'' proteins unstructured under physiologic conditions? *Proteins.* 41:415–427.
28. Li, X., P. Romero, M. Rani, A. K. Dunker, and Z. Obradovic. 1999. Predicting protein disorder for N-, C-, and internal regions. *Genome Inform. Ser. Workshop Genome Inform.* 10:30–40.
29. Bhattacharyya, R., R. P. Saha, U. Samanta, and P. Chakrabarti. 2003. Geometry of interaction of the histidine ring with other planar and basic residues. *J. Proteome Res.* 2:255–263.
30. Choi, B. O., M. S. Lee, S. H. Shin, J. H. Hwang, K. G. Choi, W. K. Kim, I. N. Sunwoo, N. K. Kim, and K. W. Chung. 2004. Mutational analysis of PMP22, MPZ, GJB1, EGR2 and NEFL in Korean Charcot-Marie-Tooth neuropathy patients. *Hum. Mutat.* 24:185–186.
31. von Heijne, G. 1990. The signal peptide. *J. Membr. Biol.* 115:195–201.
32. Kim, J., M. Mosior, L. A. Chung, H. Wu, and S. McLaughlin. 1991. Binding of peptides with basic residues to membranes containing acidic phospholipids. *Biophys. J.* 60:135–148.
33. Montich, G., S. Scarlata, S. McLaughlin, R. Lehrmann, and J. Seelig. 1993. Thermodynamic characterization of the association of small basic peptides with membranes containing acidic lipids. *Biochim. Biophys. Acta.* 1146:17–24.
34. Mosior, M., and S. McLaughlin. 1991. Peptides that mimic the pseudosubstrate region of protein kinase C bind to acidic lipids in membranes. *Biophys. J.* 60:149–159.
35. Mosior, M., and S. McLaughlin. 1992. Electrostatics and reduction of dimensionality produce apparent cooperativity when basic peptides bind to acidic lipids in membranes. *Biochim. Biophys. Acta.* 1105:185–187.
36. Peitzsch, R. M., and S. McLaughlin. 1993. Binding of acylated peptides and fatty acids to phospholipid vesicles: pertinence to myristoylated proteins. *Biochemistry.* 32:10436–10443.
37. Hartmann, E., T. A. Rapoport, and H. F. Lodish. 1989. Predicting the orientation of eukaryotic membrane-spanning proteins. *Proc. Natl. Acad. Sci. USA.* 86:5786–5790.
38. Bishop, W. R., and R. M. Bell. 1988. Assembly of phospholipids into cellular membranes: biosynthesis, transmembrane movement and intracellular translocation. *Annu. Rev. Cell Biol.* 4:579–610.

39. Op den Kamp, J. A. 1979. Lipid asymmetry in membranes. *Annu. Rev. Biochem.* 48:47–71.

40. Swierczynski, S. L., and P. J. Blackshear. 1996. Myristoylation-dependent and electrostatic interactions exert independent effects on the membrane association of the myristoylated alanine-rich protein kinase C substrate protein in intact cells. *J. Biol. Chem.* 271:23424–23430.

41. Sigal, C. T., W. Zhou, C. A. Buser, S. McLaughlin, and M. D. Resh. 1994. Amino-terminal basic residues of Src mediate membrane binding through electrostatic interaction with acidic phospholipids. *Proc. Natl. Acad. Sci. USA.* 91:12253–12257.

42. McLaughlin, S., and A. Aderem. 1995. The myristoyl-electrostatic switch: a modulator of reversible protein-membrane interactions. *Trends Biochem. Sci.* 20:272–276.

43. Eichberg, J., and S. Iyer. 1996. Phosphorylation of myelin proteins: recent advances. *Neurochem. Res.* 21:527–535.

44. Bizzozero, O. A., K. Fridal, and A. Pastuszyn. 1994. Identification of the palmitoylation site in rat myelin P0 glycoprotein. *J. Neurochem.* 62:1163–1171.

45. Sakamoto, Y., K. Kitamura, K. Yoshimura, T. Nishijima, and K. Uyemura. 1986. Fatty acid binding peptides from bovine P0 protein in peripheral nerve myelin. *Biomed. Res.* 7:261–266.

46. Iyer, S., R. Bianchi, and J. Eichberg. 2000. Tyrosine phosphorylation of PNS myelin P(0) occurs in the cytoplasmic domain and is maximal during early development. *J. Neurochem.* 75:347–354.

47. Wong, M. H., and M. T. Filbin. 1994. The cytoplasmic domain of the myelin P0 protein influences the adhesive interactions of its extracellular domain. *J. Cell Biol.* 126:1089–1097.

48. Hilmi, S., M. Fournier, H. Valeins, J. C. Gandar, and J. Bonnet. 1995. Myelin P0 glycoprotein: identification of the site phosphorylated in vitro and in vivo by endogenous protein kinases. *J. Neurochem.* 64: 902–907.

49. Yip, Y. L., H. Scheib, A. V. Diemand, A. Gattiker, L. M. Famiglietti, E. Gasteiger, and A. Bairoch. 2004. The Swiss-Prot variant page and the ModSNP database: a resource for sequence and structure information on human protein variants. *Hum. Mutat.* 23: 464–470.